



Since January 2020 Elsevier has created a COVID-19 resource centre with free information in English and Mandarin on the novel coronavirus COVID-19. The COVID-19 resource centre is hosted on Elsevier Connect, the company's public news and information website.

Elsevier hereby grants permission to make all its COVID-19-related research that is available on the COVID-19 resource centre - including this research content - immediately available in PubMed Central and other publicly funded repositories, such as the WHO COVID database with rights for unrestricted research re-use and analyses in any form or by any means with acknowledgement of the original source. These permissions are granted for free by Elsevier for as long as the COVID-19 resource centre remains active.



# Fluorescence immunoassay rapid detection of 2019-nCoV antibody based on the fluorescence resonance energy transfer between graphene quantum dots and Ag@Au nanoparticle

Nan Li<sup>a</sup>, Linhong Shi<sup>a</sup>, Xue Zou<sup>a</sup>, Tengfei Wang<sup>a</sup>, Dongmei Wang<sup>a,b</sup>, Zhengjun Gong<sup>a,b,\*</sup>, Meikun Fan<sup>a,b,\*</sup>

<sup>a</sup> Faculty of Geosciences and Environmental Engineering, Southwest Jiaotong University, Chengdu 611756, China

<sup>b</sup> State-province Joint Engineering Laboratory of Spatial Information Technology of High-Speed Rail Safety, Chengdu 611756, China

## ARTICLE INFO

### Keywords:

2019-nCoV  
Fluorescence immunosensor  
Fluorescence resonance energy transfer  
Graphene quantum dots  
Ag@AuNPs

## ABSTRACT

Severe acute respiratory syndrome coronavirus 2 (SARS-CoV-2), which has dramatically changed the world, is a highly contagious virus. The timely and accurate diagnosis of SARS-CoV-2 infections is vital for disease control and prevention. Here in this work, a fluorescence immunoassay was developed to detect 2019 Novel Coronavirus antibodies (2019-nCoV mAb). Fluorescent graphene quantum dots (GQDs) and Ag@Au nanoparticles (Ag@AuNPs) were successfully synthesized and characterized. Fluorescence resonance energy transfer (FRET) enables effective quenching of GQDs fluorescence by Ag@AuNPs. With the presence of 2019-nCoV mAb, a steric hindrance was observed between the Ag@AuNPs-NCP (2019-nCoV antigen) complex and GQDs, which reduced the FRET efficiency and restored the fluorescence of GQDs. The fluorescence enhancement efficiency has a satisfactory linear relationship with the logarithm of the 2019-nCoV mAb in a concentration range of  $0.1 \text{ pg mL}^{-1}$ – $10 \text{ ng mL}^{-1}$ , and the limit of detection was  $50 \text{ fg mL}^{-1}$ . The method has good selectivity. When the serum sample was spiked with 2019-nCoV mAb, the recovery rate was between 90.8% and 103.3%. The fluorescence immunosensor demonstrates the potential to complement the existing serological assays for COVID-19 diagnosis.

## 1. Introduction

Coronavirus disease 2019 (COVID-19) is an acute infectious disease caused by SARS-CoV-2, which is dominated by lung symptoms and can cause damage to the digestive system and nervous system. The disease can lead to the death of the patient [1]. Therefore, the effective detection of 2019-nCoV is very important. Nucleic acid testing techniques for Reverse Transcription-Polymerase Chain Reaction (RT-PCR) are clinical testing methods with the advantages of earlier detection of infection, high sensitivity and specificity [2,3]. However, the results of RT-PCR nucleic acid detection are affected by multiple factors, such as the accuracy and reproducibility of the equipment, the easy degradation of stored and transported RNA, the duration of the patient's infection, the relatively long experimental time required for sequencing, etc. [4,5]. This situation increases the risk of false negatives. It turns out that the probability of false negatives is relatively high, which is very dangerous [6,7]. Fig. 1.

It's well-known that serum-specific antibodies are another key type of choice for the diagnosis of infection. The operation of antibody detection is simple and convenient, and it does not require expensive instruments and technical personnel. In addition, it only needs to collect blood samples, which can greatly reduce the risk of infection of medical staff during specimen collection and detection. At the same time, antibody testing is convenient and quick. And it can also reduce the incidence of "false negative" test results [7,8]. It is an important means to assist nucleic acid diagnosis. Currently, serum antibody testing is used as an auxiliary method to detect 2019-nCoV [7,9–11].

Fluorescence immunoassay has received widespread attention. It has many advantages as a substitute for conventional immunoassays, such as simple operation, fast response time, high specificity and sensitivity, and good practicability [12]. In recent years, nanocomposites have attracted much attention in the field of fluorescence immunoassay [13–16]. Reports have shown that the combination of two or more nanomaterials can further tune the property for better performance in

\* Corresponding authors at: Faculty of Geosciences and Environmental Engineering, Southwest Jiaotong University, Chengdu 611756, China.  
E-mail addresses: [gzej@swjtu.edu.cn](mailto:gzej@swjtu.edu.cn) (Z. Gong), [meikunfan@gmail.com](mailto:meikunfan@gmail.com) (M. Fan).

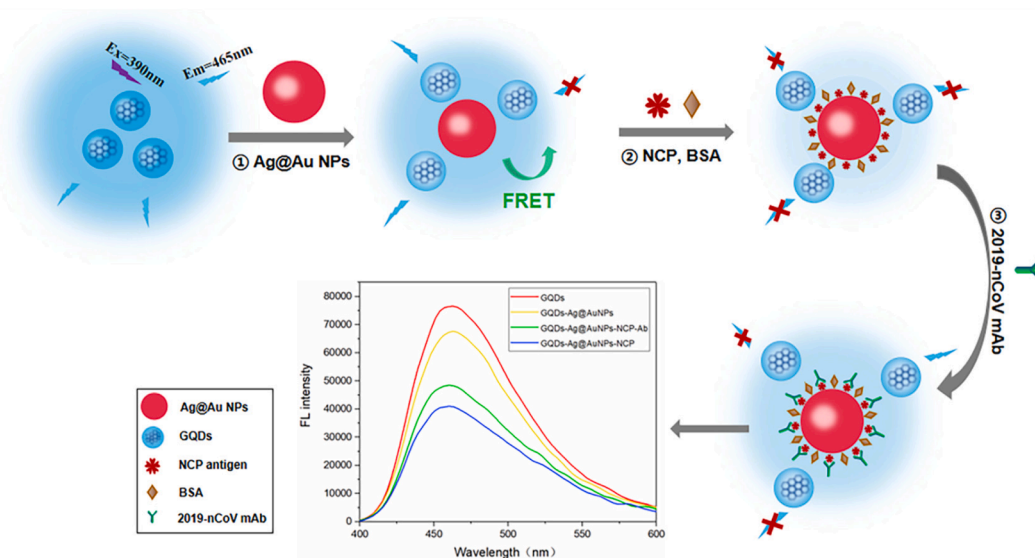


Fig. 1. Schematic representation of the detection of 2019-nCoV mAb using fluorescence immunosensor.

fluorescent immunosensor applications. Graphene quantum dot is a new type of quantum dot, which exhibits stronger edge effects than graphene. In addition, graphene quantum dots also exhibit low cytotoxicity, good water solubility, chemical inertness, stable photoluminescence, size-tunable fluorescence signatures and other properties [17–20]. These properties make them attractive fluorescent labels for the sensing of biological assays. For instance, A novel dual-mode immunoassay was designed by Zou et al. [21]. Tuberculosis (TB) antigen CFP-10 is immunoassay by using graphene quantum dots through fluorescence and surface-enhanced Raman scattering (SERS). Ag@AuNPs, a bimetallic nanomaterial, not only combines the properties of a single metal element but also has better performance than a single metal element. It enhances the stability and dispersion of the material and improves biocompatibility [22,23]. Kong et al. [24] designed a method to detect von Willebrand factor (vWF). This method also uses a complex of GQDs and Ag@AuNPs as an immunosensor.

In this work, Ag@AuNPs and GQDs were successfully synthesized. Ag@AuNPs were used as acceptors to quench the fluorescence of GQDs through FRET. Ag@AuNPs-NCP antigen was prepared with NCP antigen (2019-nCoV antigen), bovine serum albumin (BSA), and Ag@AuNPs. According to the immune response of the 2019 novel coronavirus monoclonal antibody (2019-nCoV mAb) and the influence of the steric hindrance of Ag@AuNPs-NCP and GQDs on the efficiency of FRET, the detection of 2019-nCoV mAb can be achieved with good selectivity. In this study, the preparation of GQDs and Ag@AuNPs is simple and fast. At the same time, the nanomaterial combines with the antigen through electrostatic adsorption to form a detection probe without any modification steps and simple operation. In addition, the fluorescence immunosensor has excellent optical properties and a low detection limit, falling under the clinically relevant concentration range [25].

## 2. Experimental

### 2.1. Materials and reagents

The NCP antigen (2019-nCoV antigen) was purchased from Hangzhou Yibaixin Biotechnology Co., Ltd, and the 2019 novel coronavirus monoclonal antibody (2019-nCoV mAb) was purchased from Nanjing Okay Biotechnology Co., Ltd. Citric acid (CA), sodium citrate,  $\text{HAuCl}_4 \cdot 3\text{H}_2\text{O}$ ,  $\text{AgNO}_3$ , NaOH and Bovine serum albumin (BSA) were purchased from Sinochem Reagent Co., Ltd. The buffer used for the analysis was 0.01 M phosphate-buffered saline (PBS), and all aqueous solutions were prepared in ultrapure water.

### 2.2. Equipment

Steady-state/transient fluorescence spectrometer (Edinburgh Instruments, FLS-1000, UK), JEM-2100F transmission electron microscope (TEM) (JEOL, Japan), Thermo Scientific K-Alpha+ (XPS) (ThermoFisher), USB-2000 UV-vis spectrometer (Ocean Optics, USA), electronic balance (Shanghai Sunny Hengping Scientific Instrument Co., Ltd., FA2004N), PHS-3W pH meter (Inesa, China), ultrapure water machine (Thermo Fisher, GenPure UV), three-frequency constant-temperature CNC ultrasonic cleaner (KQ-300GVDV, Kunshan Ultrasonic Instrument Factory, Jiangsu Province), magnetic heating plate (IKA Company, RCT basic),

### 2.3. Synthesis of GQDs

GQDs stock solution was prepared from pyrolytic citric acid (CA) with minor modifications as reported in the literature [26]. 2 g CA was put into a beaker and heated at 200 °C for 30 min using a heating mantle. CA gradually changed from a colorless solid to an orange liquid. Then, the orange liquid was slowly transferred to NaOH solution (100 mL, 10 mg  $\text{mL}^{-1}$ ). Finally, the GQDs solution was obtained by adjusting the pH value of GQDs to 8.0. The final product was stored at 4 °C.

### 2.4. Synthesis of Ag@AuNPs and Ag@AuNPs-NCP antigen

Ag@AuNPs were carried out using a previous method [27] with minor modifications. The total concentration of metal ions (including  $\text{HAuCl}_4$  and  $\text{AgNO}_3$ ) was maintained at 0.25 mM. First,  $\text{HAuCl}_4$  aqueous solution (0.309 mL, 30 mM) and 50 mL of ultrapure water were added to the Erlenmeyer flask and heated to boiling. Then the  $\text{AgNO}_3$  aqueous solution (0.198 mL, 20 mM) was added to the above-mixed solution. Under reflux conditions, sodium citrate solution (2.5 mL, 1%) was added and the mixed solution was heated continuously for 30 min. Finally, the solution was cooled to 25 °C under stirring conditions.

The Ag@AuNPs-NCP antigen (Ag@AuNPs-NCP) was prepared using the previous method [24] with slight modifications: First, under stirring conditions, NCP antigen (300  $\mu\text{L}$ , 5  $\mu\text{g mL}^{-1}$ ) was added to 3 mL Ag@AuNPs suspension. Then BSA solution (60  $\mu\text{L}$ , 1%) was added to block non-specific sites on the Ag@AuNPs-NCP surface. The above solution was continuously stirred at 4 °C for 4 h and centrifuged for 30 min (13,000 rpm). Finally, the sediment was ultrasonically re-dispersed in 1.5 mL PBS (pH 7.5).

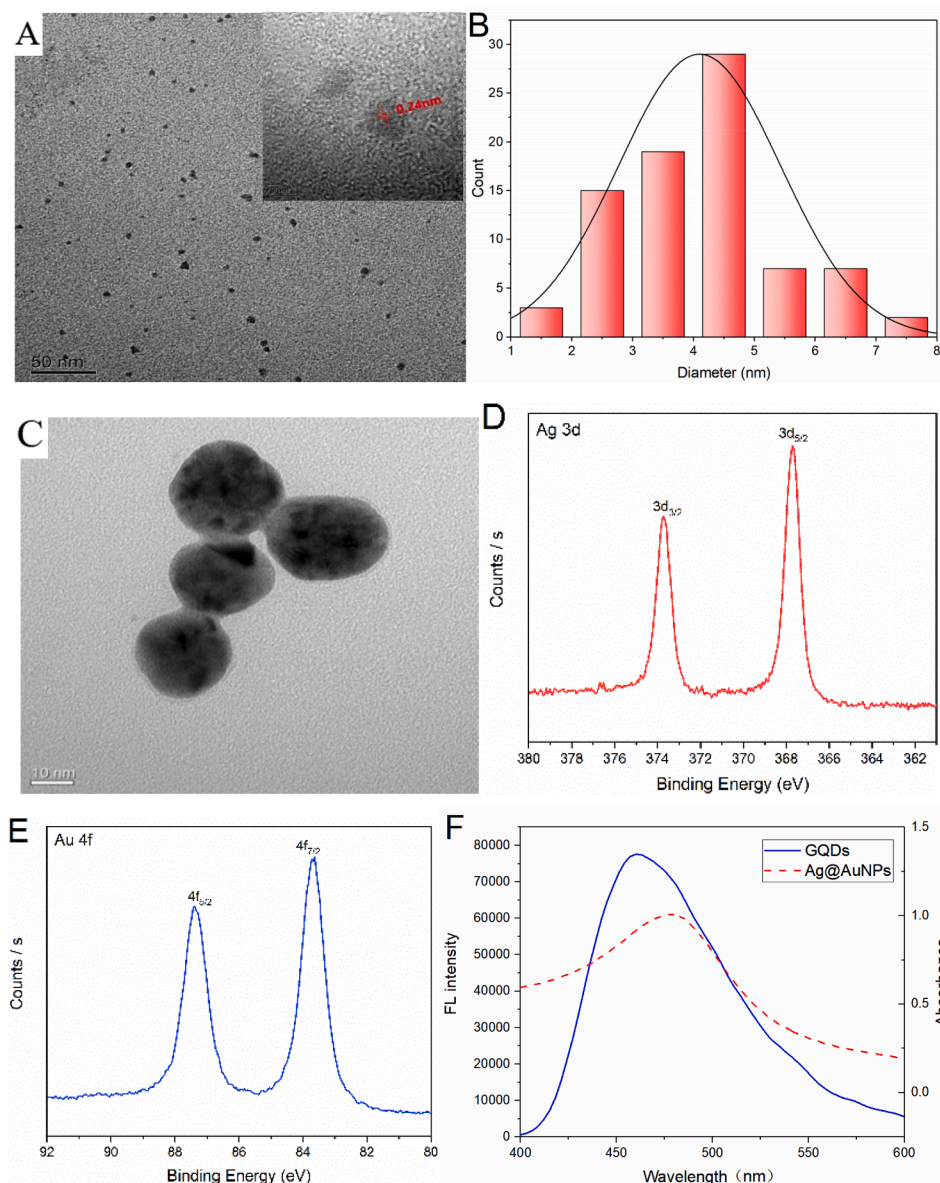


**Fig. 2.** Characterization and optical properties of GQDs and Ag@AuNPs (A) TEM and HRTEM (inset) images of GQDs. (B) Diameter distribution of the GQDs. (C) TEM image of Ag@AuNPs. (D) XPS Ag 3d spectra of the Ag@AuNPs. (E) XPS Au 4f spectra of the Ag@AuNPs. (F) UV-vis spectra of Ag@AuNPs and FL emission spectra of GQDs.

### 2.5. Detection of 2019-nCoV mAb

All experiments were performed using PBS (pH 7.5). 100  $\mu$ L Ag@AuNPs-NCP and 20  $\mu$ L 2019-nCoV mAb of different concentrations were added to a centrifuge tube to mix well, and incubated at room temperature for 150 min. Then, 20  $\mu$ L GQDs solution was added to the centrifuge tube. Finally, 160  $\mu$ L of PBS (pH 7.5) buffer solution was added to the above solution. The fluorescence spectrum of the solution was measured.

### 2.6. Detection of 2019-nCoV mAb in serum

The artificial serum was obtained from Huzhou Inno Reagents Co., Ltd and diluted 100 times with PBS (pH 7.5) before sensing. The diluted serums were spiked with known concentrations of 2019-nCoV mAb and measured under the optimum conditions.

## 3. Results and discussion

### 3.1. Characterization of GQDs and Ag@AuNPs

As shown by the TEM (Fig. 2A), the diameter of GQDs is 4–5 nm. It is nearly spherical and has good dispersibility. This is similar to the reported literature [26]. It can be seen from the HRTEM image (Inset of Fig. 2A) that the GQDs show high crystallinity with a clear lattice spacing of 0.24 nm, corresponding to (1120) lattice fringes of graphene. The TEM image (Fig. 2C) shows that Ag@AuNPs were spherical with an average grain diameter of 25 nm. This is consistent with reports in the literature [24]. The surface chemical composition of Ag@AuNPs was determined by XPS. The Ag3d spectrum can be seen in Fig. 2D. Because of the spin-orbit coupling, the binding energies are 367.7 and 373.7 eV. Its intensity ratio is 2:3, corresponding to Ag3d<sub>3/2</sub> and Ag3d<sub>5/2</sub> respectively. These are attributed to the metallic silver in Ag@AuNPs [28–31]. As plotted in Fig. 2E, there are two main peaks at 83.6 eV and 87.3 eV, corresponding to Au4f<sub>7/2</sub> and Au4f<sub>5/2</sub>, respectively. This proves the

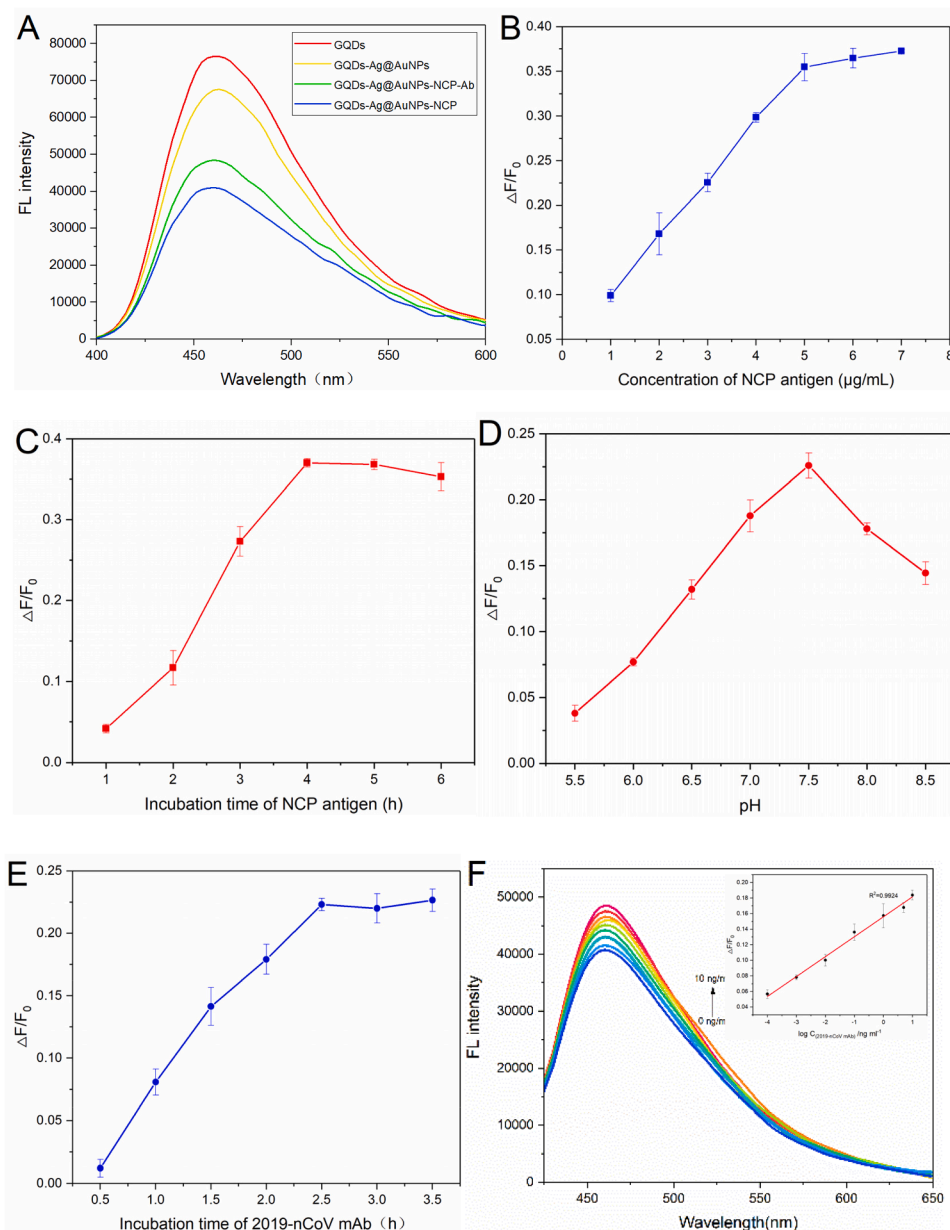


**Fig. 3.** Optimize detection conditions and detect 2019-nCoV mAb. (A) Fluorescence comparison of GQDs, GQDs + Ag@AuNPs, GQDs + Ag@AuNPs-NCP and GQDs + Ag@AuNPs-NCP + 2019-nCoV mAb. (B) The influence of concentration of NCP antigen. (C) The influence of incubation time of NCP antigen. (D) The influence of pH on the reaction system. (E) The influence of the incubation time of 2019-nCoV mAb on the reaction system. (F) Fluorescence spectra of the mixture of GQDs and Ag@AuNPs-NCP with different concentrations of 2019-nCoV mAb. (0–10  $\text{ng mL}^{-1}$ ). Inset: The relationship between the fluorescence enhancement efficiency and the logarithm of 2019-nCoV mAb concentration ( $\lg C_{2019\text{-nCoV mAb}}$ ).

existence of metallic gold. The observed position is consistent with those reported in the literature [28–30,32]. The Raman spectrum of GQDs in Fig. S1 shows two characteristic peaks located at  $1340\text{ cm}^{-1}$  and  $1609\text{ cm}^{-1}$ , which correspond to the characteristic D and G bands of carbon materials, respectively.[33,34]

In addition, in order to study the optical properties of GQDs, the obtained GQDs were characterized by UV–Vis spectroscopy. The blue line in Fig. S2 is the UV–Vis spectrum of graphene quantum dots. The prepared GQDs show an obvious  $\pi\text{-}\pi^*$  absorption peak at 365 nm, which is related to the C = C transition in the UV–Vis spectrum [35]. At the same time, Ag@AuNPs have an obvious absorption peak near 490 nm, which is blue-shifted compared to that of AuNPs at 523 nm (Fig. S3) [27]. As shown in Fig. S4, the UV–Vis spectrum was used to characterize Ag@AuNPs-NCP. Compared with the original Ag@AuNPs, Ag@AuNPs-NCP shows a significant absorbance near 280 nm, which is derived from the NCP antigen. The results showed that Ag@AuNPs-NCP probe was successfully fabricated. The fluorescence emission spectrum of graphene quantum dots was given in Fig. 2F. In addition, the excitation wavelength of GQDs ranges from 340 nm to 420 nm, and the emission

wavelength is red-shifted by about 10 nm (Fig. S5), indicating that GQDs hardly depends on the fluorescence characteristics of excitation. When the excitation wavelength is 390 nm, the graphene quantum dots has a maximum emission at 465 nm. This is consistent with reports in the literature [36], indicating that GQDs were successfully synthesized.

### 3.2. Mechanism of detecting 2019-nCoV mAb

The first condition for FRET to occur is that there is a significant overlap between the absorption spectrum of the acceptor and the emission spectra of the donor. This allows the acceptor to absorb the energy released by the donor. Secondly, the fluorescent chromophores of the donor and acceptor must be arranged in an appropriate way, because the dipole has a certain spatial orientation. In addition, the donor and acceptor must be close enough, but the distance needs to exceed the collision diameter between them. In this case, FRET may occur [37]. The fluorescence emission peaks of GQDs can overlap with the absorption spectra of some receptors because their emission spectra are usually in the visible light region.

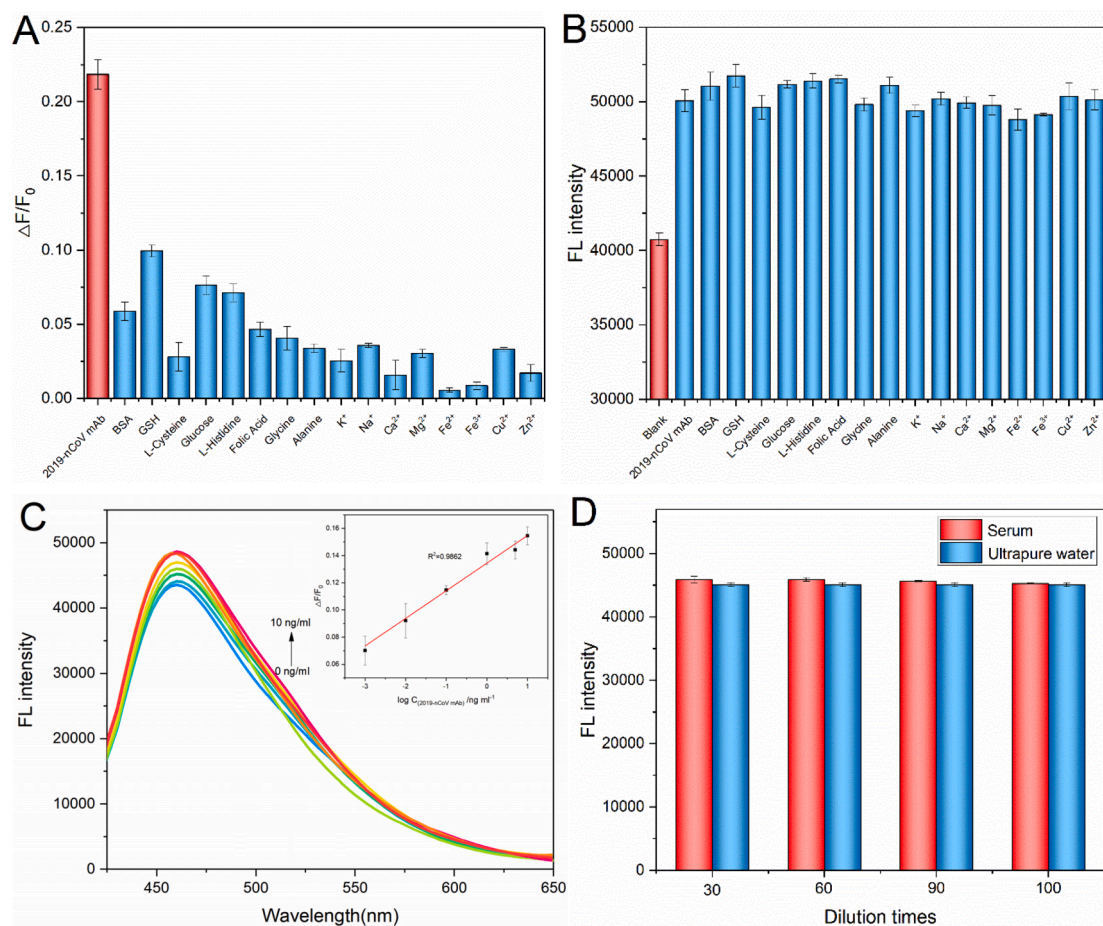


**Fig. 4.** Selectivity and its detection of 2019-nCoV mAb in serum (A) Selective experiments for 2019-nCoV detection (B) The fluorescence intensities of the probe to 2019-nCoV mAb in the presence of interfering substance. (C) Fluorescence spectra of the mixture of GQDs and Ag@AuNPs-NCP in artificial serum with different concentrations of 2019-nCoV mAb. (0–10 ng mL<sup>-1</sup>). Inset: The relationship between the fluorescence enhancement efficiency and the logarithm of 2019-nCoV mAb concentration (lgC<sub>2019-nCoV mAb</sub>). (D) Comparison of fluorescence emission spectra of GQDs from a mixture of Ag@AuNPs-NCP and 2019-nCoV mAb (0.1 ng mL<sup>-1</sup>) in diluted artificial serum and ultrapure water.

The fluorescence emission spectra of 2019-nCoV mAb is shown in Fig. 3A. It can be seen that GQDs (red line) has the highest fluorescence emission peak at 465 nm. In the presence of Ag@AuNPs, the fluorescence intensity was reduced to a certain extent. At the same time, GQDs have a strong UV absorption peak at 365 nm, while Ag@AuNPs have a significant peak at 490 nm, as given in the absorption spectrum (Fig. S2). In the figure, it can be clearly seen that the sum of the absorbance of GQDs and Ag@AuNPs (red line) is greater than the absorption peak of the mixture containing GQDs and Ag@AuNPs (green line), which indicates that there is an interaction between them. The fluorescence emission spectra of GQDs partially overlap with the UV absorption spectrum of Ag@AuNPs. The main conclusion that can be drawn is that there is FRET between them, [38] where GQDs are donors and Ag@AuNPs are acceptors. In order to further confirm the FRET mechanism, the fluorescence lifetime of GQDs without Ag@AuNPs and GQDs with Ag@AuNPs were measured by a steady-state/transient fluorescence spectrometer (Fig. S6). In the presence of Ag@AuNPs, the average lifetime of GQDs is reduced from 5.75 ns to 2.64 ns. It can be inferred from the above results that the fluorescence quenching of GQDs is based on the principle of FRET. It can be seen from the detection diagram that the immobilization of BSA and NCP antigen on Ag@AuNPs makes the distance between Ag@AuNPs-NCP and GQDs farther until the optimal distance for FRET is reached [39]. The FRET efficiency reaches maximum value, and the fluorescence intensity of GQDs is further reduced. When Ag@AuNPs-NCP and 2019-nCoV mAb exist at the same time, the distance between 2019-nCoV mAb-nanocomposites and GQDs

is further increased due to the steric-hindrance effect. At the same time, the efficiency of FRET decreases, and the fluorescence of GQDs turns on.

### 3.3. Optimization of detection conditions

In order to obtain excellent detection performance, the relevant experimental conditions were optimized, including the ratio of the concentration of Au to Ag in Ag@AuNPs, the ratio of GQDs to Ag@AuNPs, the concentration and reaction time of NCP antigen when preparing Ag@AuNPs-NCP, the pH conditions of detection, and the incubation time of 2019-nCoV mAb and Ag@AuNPs-NCP. In addition, AgNPs have been reported to be able to denature proteins [40]. Therefore, Ag@AuNPs were selected to combine with NCP antigen to prepare probes. According to the absorption spectrum of Ag@AuNPs with various concentration ratios of Au and Ag (Fig. S3), it can be seen that when Au: Ag = 7:3, the overlap area of the absorption spectrum and the fluorescence emission spectrum of GQDs is the largest. And it has the best fluorescence quenching effect on GQDs (Fig. S2). As shown in Fig. S8, Ag@AuNPs with a volume of 100  $\mu$ L were selected for the experiment. The concentration of NCP antigen and the incubation time when preparing the Ag@Au NPs-NCP probe was examined. The fluorescence intensity of GQDs containing Ag@AuNPs-NCP was denoted by  $F_0$ . The fluorescence intensity of GQDs containing both 2019-nCoV mAb and Ag@AuNPs-NCP was represented by  $F_1$ . And their difference between  $\Delta F$  ( $\Delta F = F_0 - F_1$ ) and the ratio of  $\Delta F$  to  $F_0$  was calculated. It can be seen that the optimal concentration of NCP antigen is 5  $\mu$ g mL<sup>-1</sup>

(Fig. 4B), and the optimal incubation time is 4 h (Fig. 4C). In addition, the influence of pH was studied in the range of pH 5.5–8.5 (Fig. 3D). When the pH values of the solution reach 7.5, the fluorescence enhancement of the as-developed probe displays the maximum. And the value of  $\Delta F/F_0$  decreased under both acidic or alkaline conditions. According to a previous report [41], the stability of the biological activity of the immobilized protein is dependent on the pH of the solution. Acidic and alkaline conditions will reduce protein activity and cause a significant decrease in the performance of the immunosensor. The effect of incubation time on the reaction system was shown in Fig. 3E. With the increase of incubation time,  $\Delta F/F_0$  gradually increased and stabilized after 2.5 h. It can be seen that further incubation time will not improve the sensitivity. Therefore, this study chose the optimal incubation time of Ag@AuNPs-NCP and 2019-nCoV as 2.5 h.

### 3.4. Detection of 2019-nCoV mAb

Under the optimum conditions, the fluorescence intensity of Ag@AuNPs-NCP and GQDs containing different concentrations of 2019-nCoV mAb ( $0, 1 \times 10^{-4}, 1 \times 10^{-3}, 1 \times 10^{-2}, 0.1, 1, 2, 5$  and  $10 \text{ ng mL}^{-1}$ ) was recorded. From Fig. 3F, it can be seen that the fluorescence of GQDs gradually recovered as the concentration of 2019-nCoV mAb increased. This probably indicated that more 2019-nCoV mAb was combined with Ag@AuNPs. In this case, Ag@AuNPs and GQDs gradually separate, and the fluorescence of GQDs gradually recovered. The fluorescence enhancement efficiency ( $\Delta F/F_0$ ) has a linear relationship with the logarithm of the 2019-nCoV mAb concentration within the range of  $0.1 \text{ pg mL}^{-1}$ – $10 \text{ ng mL}^{-1}$ . The regression equation is  $\Delta F/F_0 = 0.0225 \lg c_{2019\text{-nCoV mAb}} + 0.1563$ . The correlation coefficient is 0.9924, indicating a strong linear correlation. The detection limit is calculated to be  $50 \text{ fg mL}^{-1}$ , falling under the clinically relevant concentration range. [42,43]

### 3.5. Specificity, stability and reproducibility

In order to verify selectivity in the presence of interferences, potential coexisting components in serum are also tested. These coexisting ingredients include BSA, GSH (glutathione), L-cysteine, glucose, L-histidine, folic acid, glycine, alanine and some inorganic ions. The fluorescence intensity of GQDs containing Ag@AuNPs-NCP was recorded. And on this basis, 2019-nCoV mAb ( $10 \text{ ng mL}^{-1}$ ) and the above components ( $100 \text{ ng mL}^{-1}$ ) were added separately for detection. It can be seen from Fig. 4A, the fluorescence intensity of the 2019-nCoV mAb fluorescent immunosensor is greater than that of the negative control. And the detection system is less affected by the interfering substances (Fig. 4B). Therefore, this system has good selectivity. In addition, the stability of the probe was evaluated by measuring the fluorescence intensity of GQDs-Ag@AuNPs-NCP (Fig. S9). This probe retained 99.0%, 97.8%, and 97.0% of its initial intensity after GQDs-Ag@AuNPs-NCP was kept in the refrigerator at  $4 \text{ }^\circ\text{C}$  for 5 days, 10 days and 15 days, respectively. Therefore, the stability of the probe is acceptable. The reproducibility was studied by detecting  $0.1 \text{ ng mL}^{-1}$  2019-nCoV mAb with 5 different batches of probes. The relative standard deviation was 4.5%. The experimental results indicated that the probe displayed good reproducibility.

### 3.6. Determination of 2019-nCoV mAb in artificial serum

This method was further used for the detection of 2019-nCoV mAb in artificial serum. In this process, a series of samples are prepared by adding different concentrations of 2019-nCoV mAb ( $0, 1 \times 10^{-3}, 1 \times 10^{-2}, 0.1, 1, 2, 5$  and  $10 \text{ ng mL}^{-1}$ ) to the diluted serum samples. It can be seen from Fig. 4C, fluorescence enhancement efficiency ( $\Delta F/F_0$ ) has a satisfactory linear relationship with the logarithm of the 2019-nCoV mAb concentration within the scope of  $1 \text{ pg mL}^{-1}$ – $10 \text{ ng mL}^{-1}$  when serum was diluted by 30 times. The regression equation is  $\Delta F/F_0 = 0.0211 \lg c_{2019\text{-nCoV mAb}} + 0.1345$ , the  $R^2$  is 0.9862 and the LOD is  $0.40 \text{ pg mL}^{-1}$ . When the serum is diluted approximately 30 times, the initial fluorescence without antibodies is greater than the fluorescence intensity in ultrapure water. Through the comparison of different dilution times of serum (Fig. 4D), it can be seen that when the dilution times are 100 times, the fluorescence intensity of 2019-nCoV mAb in serum was closer to the fluorescence intensity in ultrapure water, and the recovery rate was better. Therefore, in order to reduce the matrix effect [44], the serum was diluted 100 times and samples of standard 2019-nCoV mAb containing 1, 0.1, and  $0.01 \text{ ng mL}^{-1}$  were prepared for testing. The recovery ranged from 90.8% to 103.3% with relative standard deviations (RSD) less than 10.3% (Table 1). The method showed good accuracy in the detection of 2019-nCoV mAb in artificial serum.

**Table 1**

Recovery of 2019-nCoV mAb in serum samples by using the proposed method ( $n = 3$ ).

Samples	Added ( $\text{ng mL}^{-1}$ )	Found ( $\text{ng mL}^{-1}$ )	Recovery (%)	RSD (%)
1	1.0	0.9080	90.79	9.70
2	0.1	0.1028	102.8	6.90
3	0.01	0.0103	103.3	10.3

$F_0 = 0.0211 \lg c_{2019\text{-nCoV mAb}} + 0.1345$ , the  $R^2$  is 0.9862 and the LOD is  $0.40 \text{ pg mL}^{-1}$ . When the serum is diluted approximately 30 times, the initial fluorescence without antibodies is greater than the fluorescence intensity in ultrapure water. Through the comparison of different dilution times of serum (Fig. 4D), it can be seen that when the dilution times are 100 times, the fluorescence intensity of 2019-nCoV mAb in serum was closer to the fluorescence intensity in ultrapure water, and the recovery rate was better. Therefore, in order to reduce the matrix effect [44], the serum was diluted 100 times and samples of standard 2019-nCoV mAb containing 1, 0.1, and  $0.01 \text{ ng mL}^{-1}$  were prepared for testing. The recovery ranged from 90.8% to 103.3% with relative standard deviations (RSD) less than 10.3% (Table 1). The method showed good accuracy in the detection of 2019-nCoV mAb in artificial serum.

## 4. Conclusions

A new type of 2019-nCoV antibody fluorescence immunoassay method combining GQDs and Ag@AuNPs is proposed. This study prepared fluorescent GQDs and used them as fluorescent probes. The prepared Ag@AuNPs were spherical with an average grain diameter of 25 nm. Due to FRET, Ag@AuNPs suppressed the fluorescence of GQDs. When Ag@AuNPs-NCP coexisted with 2019-nCoV mAb, the efficiency of FRET was decreased because of the steric-hindrance effect. At this time, the fluorescence of GQDs was turned on. This fluorescent probe exhibits high sensitivity and selectivity. In addition, this probe has been successfully applied to artificial serum samples, which validated the efficiency of the proposed probe for detecting 2019-nCoV mAb in complex samples. This method of antibody detection provides another possibility for 2019-nCoV detection.

### CRediT authorship contribution statement

**Nan Li:** Data curation, Writing – original draft. **Linhong Shi:** Data curation, Writing – original draft. **Xue Zou:** Conceptualization, Investigation, Methodology, Writing – original draft. **Tengfei Wang:** Conceptualization, Supervision, Writing – review & editing. **Dongmei Wang:** Supervision. **Zhengjun Gong:** Conceptualization, Supervision, Writing – review & editing. **Meikun Fan:** Conceptualization, Supervision, Writing – review & editing.

### Declaration of Competing Interest

The authors declare that they have no known competing financial interests or personal relationships that could have appeared to influence the work reported in this paper.

### Acknowledgements

The author would like to thank for the financial support of the National Natural Science Foundation of China (Nos. 21777131 & 22176154) and the Fundamental Research Funds for the Central Universities (No. A0920502052001-6). We would like to thank the Analytical and Testing Center of Southwest Jiaotong University for the experimental conditions.

## Appendix A. Supplementary data

Supplementary data to this article can be found online at <https://doi.org/10.1016/j.microc.2021.107046>.

## References

- [1] Y.S. Malik, S. Sircar, S. Bhat, K. Sharun, K. Dhama, M. Dadar, R. Tiwari, W. Chaicumpa, Emerging novel coronavirus (2019-nCoV)-current scenario, evolutionary perspective based on genome analysis and recent developments, *Vet. Q.* 40 (1) (2020) 68–76.
- [2] D.K.W. Chu, Y. Pan, S.M.S. Cheng, K.P.Y. Hui, P. Krishnan, Y. Liu, D.Y.M. Ng, C.K. C. Wan, P. Yang, Q. Wang, M. Peiris, L.L.M. Poon, Molecular diagnosis of a novel coronavirus (2019-nCoV) causing an outbreak of pneumonia, *Clin. Chem.* 66 (2020) 549–555.
- [3] B. Giri, S. Pandey, R. Shrestha, K. Pokharel, F.S. Ligler, B.B. Neupane, Review of analytical performance of COVID-19 detection methods, *Anal. Bioanal. Chem.* 413 (1) (2021) 35–48.
- [4] A. Khan, B. Wilson, I.M. Gould, Current and future treatment options for community-associated MRSA infection, *Expert Opin. Pharmacother.* 19 (5) (2018) 457–470.
- [5] M. Shen, Y. Zhou, J. Ye, A.A. Abdullah AL-maskri, Y.u. Kang, S.u. Zeng, S. Cai, Recent advances and perspectives of nucleic acid detection for coronavirus, *J. Pharm. Anal.* 10 (2) (2020) 97–101.
- [6] A. Tahamtan, A. Ardebili, Real-time RT-PCR in COVID-19 detection: issues affecting the results, *Expert Rev Mol Diagn* 20 (5) (2020) 453–454.
- [7] P. Rai, B.K. Kumar, V.K. Deekshit, I. Karunasagar, I. Karunasagar, Detection technologies and recent developments in the diagnosis of COVID-19 infection, *Appl. Microbiol. Biotechnol.* 105 (2) (2021) 441–455.
- [8] C.Y.P. Lee, R.T.P. Lin, L. Renia, L.F.P. Ng, Serological approaches for COVID-19: epidemiologic perspective on surveillance and control, *Immunology* 11 (2020) 1–7.
- [9] F. Xiang, X. Wang, X. He, Z. Peng, B. Yang, J. Zhang, Q. Zhou, H. Ye, Y. Ma, H. Li, X. Wei, P. Cai, W.L. Ma, Antibody detection and dynamic characteristics in patients with coronavirus disease 2019, *Clin. Infect. Dis.* 71 (2020) 1930–1934.
- [10] T. Ji, Z. Liu, G. Wang, X. Guo, S. Akbar khan, C. Lai, H. Chen, S. Huang, S. Xia, B. o. Chen, H. Jia, Y. Chen, Q. Zhou, Detection of COVID-19: A review of the current literature and future perspectives, *Biosens. Bioelectron.* 166 (2020) 112455, <https://doi.org/10.1016/j.bios.2020.112455>.
- [11] S.A. Ejazi, S. Ghosh, N. Ali, Antibody detection assays for COVID-19 diagnosis: an early overview, *Immunol. Cell Biol.* 99 (1) (2021) 21–33.
- [12] Y.-W. Wang, L. Chen, M. Liang, H. Xu, S. Tang, H.-H. Yang, H. Song, Sensitive fluorescence immunoassay of alpha-fetoprotein through copper ions modulated growth of quantum dots in-situ, *Sens. Actuators, B* 247 (2017) 408–413.
- [13] J. Hu, X. Hou, P. Wu, Ultrasensitive atomic fluorescence spectrometric detection of DNA with quantum dot-assemblies as signal amplification labels, *J. Anal. At. Spectrom.* 30 (4) (2015) 888–894.
- [14] S. Yektaniroumand Digehsaraei, M. Salouti, B. Amini, S. Mahmazi, M. Kalantari, A. Kazemzadeh, J. Mehrvand, Developing a fluorescence immunosensor for detection of HER2-positive breast cancer based on graphene and magnetic nanoparticles, *Microchem. J.* 167 (2021), 106300.
- [15] P.R. Aranda, G.A. Messina, F.A. Bertolino, S.V. Pereira, M.A. Fernández Baldo, J. Raba, Nanomaterials in fluorescent laser-based immunosensors: Review and applications, *Microchem. J.* 141 (2018) 308–323.
- [16] X. Liu, R. Liu, Y. Tang, L. Zhang, X. Hou, Y. Lv, Antibody-biotemplated HgS nanoparticles: extremely sensitive labels for atomic fluorescence spectrometric immunoassay, *Analyst* 137 (2012) 1473–1480.
- [17] L. Li, G. Wu, G. Yang, J. Peng, J. Zhao, J.-J. Zhu, Focusing on luminescent graphene quantum dots: current status and future perspectives, *Nanoscale* 5 (2013) 4015–4039.
- [18] Z. Zhang, J. Zhang, N. Chen, L. Qu, Graphene quantum dots: an emerging material for energy-related applications and beyond, *Energy Environ. Sci.* 5 (2012) 8869–8890.
- [19] J. Shen, Y. Zhu, X. Yang, C. Li, Graphene quantum dots: emergent nanolights for bioimaging, sensors, catalysis and photovoltaic devices, *Chem. Commun.* 48 (2012) 3686–3699.
- [20] Z.G. Khan, P.O. Patil, A comprehensive review on carbon dots and graphene quantum dots based fluorescent sensor for biothiols, *Microchem. J.* 157 (2020), 105011.
- [21] F. Zou, H. Zhou, T.V. Tan, J. Kim, K. Koh, J. Lee, Dual-mode SERS-fluorescence immunoassay using graphene quantum dot labeling on one-dimensional aligned magnetoplasmonic nanoparticles, *ACS Appl. Mater. Interfaces* 7 (22) (2015) 12168–12175.
- [22] S. Guha, S. Roy, A. Banerjee, Fluorescent Au@Ag core-shell nanoparticles with controlled shell thickness and Hg(II) sensing, *Langmuir* 27 (21) (2011) 13198–13205.
- [23] O.J. Achadu, I. Uddin, T. Nyokong, The interaction between graphene quantum dots grafted with polyethyleneimine and Au@Ag nanoparticles: Application as a fluorescence “turn-on” nanoprobe, *J. Photochem. Photobiol., A* 324 (2016) 96–105.
- [24] L. Kong, Y. Li, C. Ma, B. Liu, L. Tan, Sensitive immunoassay of von Willebrand factor based on fluorescence resonance energy transfer between graphene quantum dots and Ag@Au nanoparticles, *Colloids Surf. B* 165 (2018) 286–292.
- [25] R. Funari, K.-Y. Chu, A.Q. Shen, Detection of antibodies against SARS-CoV-2 spike protein by gold nanospikes in an opto-microfluidic chip, *Biosens. Bioelectron.* 169 (2020), 112578.
- [26] Y. Dong, J. Shao, C. Chen, H. Li, R. Wang, Y. Chi, X. Lin, G. Chen, Blue luminescent graphene quantum dots and graphene oxide prepared by tuning the carbonization degree of citric acid, *Carbon* 50 (12) (2012) 4738–4743.
- [27] Y. Sun, Y. Xia, Gold and silver nanoparticles: a class of chromophores with colors tunable in the range from 400 to 750 nm, *Analyst* 128 (2003) 686–691.
- [28] D.i. Li, L. Meng, S. Dang, D. Jiang, W. Shi, Hydrogen peroxide sensing using Cu<sub>2</sub>O nanocubes decorated by Ag-Au alloy nanoparticles, *J. Alloy. Compd.* 690 (2017) 1–7.
- [29] S. Pedireddy, A. Li, M. Bosman, I.Y. Phang, S. Li, X.Y. Ling, Synthesis of spiky Ag-Au octahedral nanoparticles and their tunable optical properties, *J. Phys. Chem. C* 117 (32) (2013) 16640–16649.
- [30] R.C. Rodriguez, H. Troiani, S.E. Moya, M.M. Bruno, P.C. Angelomé, Bimetallic Ag-Au nanoparticles inside mesoporous titania thin films: synthesis by photoreduction and galvanic replacement, and catalytic activity, *Eur. J. Inorg. Chem.* 2020 (2020) 568–574.
- [31] L.i. Zhang, C. Wang, Y.i. Zhang, A facile strategy to synthesize bimetallic Au/Ag nanocomposite film by layer-by-layer assembly technique, *Appl. Surf. Sci.* 258 (14) (2012) 5312–5318.
- [32] M. Martins, B. Šljukić, Ö. Metin, M. Sevim, C.A.C. Sequeira, T. Şener, D.M. F. Santos, Bimetallic PdM (M = Fe, Ag, Au) alloy nanoparticles assembled on reduced graphene oxide as catalysts for direct borohydride fuel cells, *J. Alloy. Compd.* 718 (2017) 204–214.
- [33] D.K. Nguyen, T. Kim, Graphene quantum dots produced by exfoliation of intercalated graphite nanoparticles and their application for temperature sensors, *Appl. Surf. Sci.* 427 (2018) 1152–1157.
- [34] S. Li, Y. Li, J. Cao, J. Zhu, L. Fan, X. Li, Sulfur-doped graphene quantum dots as a novel fluorescence probe for highly selective and sensitive detection of Fe<sup>3+</sup>, *Anal. Chem.* 86 (20) (2014) 10201–10207.
- [35] Q. Liu, B. Guo, Z. Rao, B. Zhang, J.R. Gong, Strong two-photon-induced fluorescence from photostable, biocompatible nitrogen-doped graphene quantum dots for cellular and deep-tissue imaging, *Nano Lett.* 13 (6) (2013) 2436–2441.
- [36] S. Weng, D. Liang, H. Qiu, Z. Liu, Z. Lin, Z. Zheng, A. Liu, W. Chen, X. Lin, A unique turn-off fluorescence strategy for sensing dopamine based on formed polydopamine (pDA) using graphene quantum dots (GQDs) as fluorescent probe, *Sens. Actuators, B* 221 (2015) 7–14.
- [37] H. Sahoo, Förster resonance energy transfer – A spectroscopic nanoruler: Principle and applications, *J. Photochem. Photobiol., C* 12 (1) (2011) 20–30.
- [38] W. Fu, H. Wang, Y. Chen, J. Ding, G. Shan, Fluorescence sensing analysis for rapid detection of serum glutathione based on degrading AuNCs@Lys-MnO<sub>2</sub> fluorescence resonance energy transfer system, *Microchem. J.* 159 (2020), 105556.
- [39] H. Yang, C. Hao, H. Liu, K. Zhong, R. Sun, Influence of bovine hemoglobin on the disruption of fluorescence resonance energy transfer between zinc sulfide quantum dots and fluorescent silica nanoparticles, *J. Mol. Liq.* 332 (2021), 115851.
- [40] C. Zhang, J. Huang, X. Lan, H. Qi, D. Fan, L. Zhang, Synergy of bioinspired chimeric protein and silver nanoparticles for fabricating “kill-release” antibacterial coating, *Appl. Surf. Sci.* 557 (2021), 149799.
- [41] J.-D. Qiu, R.-P. Liang, R. Wang, L.-X. Fan, Y.-W. Chen, X.-H. Xia, A label-free amperometric immunosensor based on biocompatible conductive redox chitosan-ferrocene/gold nanoparticles matrix, *Biosens. Bioelectron.* 25 (4) (2009) 852–857.
- [42] J.F. Brown, J.M. Dye, S. Tozay, G. Jeh-Mulbah, D.A. Wohl, W.A. Fischer, 2nd, C.K. Cunningham, K. Rowe, P. Zacharias, J. van Hasselt, D.A. Norwood, N.M. Thielman, S.E. Zak, D.L. Hoover, Anti-Ebola virus antibody levels in convalescent plasma and viral load after plasma infusion in patients with ebola virus disease, *J. Inf. Dis.* 218 (2018) 555–562.
- [43] Q.-X. Long, B.-Z. Liu, H.-J. Deng, G.-C. Wu, K. Deng, Y.-K. Chen, P.u. Liao, J.-F. Qiu, Y. Lin, X.-F. Cai, D.-Q. Wang, Y. Hu, J.-H. Ren, N.i. Tang, Y.-Y. Xu, L.-H. Yu, Z. Mo, F. Gong, X.-L. Zhang, W.-G. Tian, L. Hu, X.-X. Zhang, J.-L. Xiang, H.-X. Du, H.-W. Liu, C.-H. Lang, X.-H. Luo, S.-B. Wu, X.-P. Cui, Z. Zhou, M.-M. Zhu, J. Wang, C.-J. Xue, X.-F. Li, L.i. Wang, Z.-J. Li, K. Wang, C.-C. Niu, Q.-J. Yang, X.-J. Tang, Y. Zhang, X.-M. Liu, J.-J. Li, D.-C. Zhang, F. Zhang, P. Liu, J. Yuan, Q. Li, J.-L. Hu, J. Chen, A.-L. Huang, Antibody responses to SARS-CoV-2 in patients with COVID-19, *Nat. Med.* 26 (6) (2020) 845–848.
- [44] Z. Zou, D. Du, J. Wang, J.N. Smith, C. Timchalk, Y. Li, Y. Lin, Quantum dot-based immunochromatographic fluorescent biosensor for biomonitoring trichloropyridinol, a biomarker of exposure to chlorpyrifos, *Anal. Chem.* 82 (12) (2010) 5125–5133.